MINERALOGICAL, MICROSTRUCTURAL AND COMPRESSIVE STRENGTH CHARACTERIZATION OF FLY ASH AS MATERIALS IN GEOPOLYMER CEMENT

Cut Rahmawati[*], Sri Aprilia[**], Taufiq Saidi[**], Teuku Budi Aulia[**]

[*]*Doctoral Program, School of Engineering, Universitas Syiah Kuala, Banda Aceh, Indonesia,*
cut_19@mhs.unsyiah.ac.id
[**]*Doctoral Program, School of Engineering, Universitas Syiah Kuala, Banda Aceh, Indonesia,*
Department of Chemical Engineering, Universitas Syiah Kuala, Banda Aceh, Indonesia,
sriaprilia@unsyiah.ac.id, taufiq_saidi@unsyiah.ac.id, aulia@unsyiah.ac.id

Email Correspondence : sriaprilia@unsyiah.ac.id

Abstract: This study was designed to examine the mineral, microstructural, and mechanical strength properties of fly ash and its feasibility as a raw material for geopolymer cement. The study used an experimental method by examining the characteristics of fly ash by X-ray Fluorescence Spectrometer (XRF), Fourier transform infrared (FTIR) spectroscopy, X-ray diffraction (XRD), hydrometer method, Scanning electron microscopy (SEM), and compressive strength testing. For creating the geopolymer cement paste, a concentration of NaOH 10M was used, with a ratio of water/solid = 0.4 and a ratio of $Na_2SiO_3/NaOH = 1$ using curring at room temperature. The results showed the geopolymer pastes have a compressive strength of 18.1 MPa and 21.5 MPa after 7 days and 28 days. The XRD results showed a decrease in the peak of 2θ at 26.54° because the amorphous part had transformed into a C-S-H solution in geopolymer cement. This finding was supported by the FTIR spectra results showing Si-O-Si bending vibration and the functional group of AlO_2. It showed that Nagan Raya fly ash-based geopolymer is a potential construction material.
Keywords: geopolymer, fly ash, epoxy, cement, compressive strength

Abstrak: Penelitian ini dirancang untuk mendapatkan sifat mineral, mikrostruktural, dan kekuatan mekanis dari *fly ash* serta kesesuaiannya sebagai material dasar pada semen geopolimer. Metode penelitian yang digunakan adalah metode eksperimen dengan cara menguji karakteristik dari *fly ash* dengan pengujian *X-ray Fluorescense Spectrometer* (XRF), *Fourier transform infrared* (FTIR) *spectoscopy, X-ray diffraction* (XRD), *hydrometer method, Scanning electron microscopy* (SEM) dan kuat tekan. Untuk pembuatan pasta semen geopolimer digunakan konsentrasi NaOH 10 M, rasio *water/solid* 0,4 dan rasio $Na_2SiO_3/NaOH = 1$ dengan perawatan pada suhu kamar. Hasil menunjukkan setelah 7 hari pasta geopolimer memiliki kuat tekan 18,1 MPa dan 21,5 MPa pada 28 hari. Hasil XRD menunjukkan adanya penurunan puncak 2θ pada 26,54° ini disebabkan karena bagian *amorf* dari *fly ash* telah menjadi larutan C-S-H pada semen geopolimer. Hasil ini diperkuat dengan analisis FTIR *spectra* yang menunjukkan adanya Si-O-Si *bending vibration* dan gugus fungsi dari AlO_2. Hasil menunjukkan *fly ash* dari Nagan Raya potensial sebagai bahan material konstruksi berbasis geopolimer.
Kata kunci : geopolimer, *fly ash*, *epoxy*, semen, kuat tekan

Introduction

The use of portland cement (PC) as the critical binder material in concrete creates many environmental concerns because of its energy consumption and carbon dioxide (CO_2) emissions. Depending on the power station, the output of one ton of cement is expected to release between 0.7 and 1.0 tons of CO_2 (Davidovits, 1991) (Peng et al., 2013). Therefore it is important to look for other materials that are more environmentally friendly, and that can replace cement.

The application of sustainable cementitious materials replacing the Portland cement in the building industry will considerably contribute to the relief of the environmental problems related to CO_2 emission and global warming. Geopolymer concrete (GPC) is a sustainable cement-less concrete prepared using industrial by-product materials, such as slag, fly ash, and other waste. Previous studies showed that the GPC has better mechanical properties than OPC concrete, the durability performance is a crucial concern for its application in infrastructure.

In the geopolymeric reaction, silica and alumina in the fly ash react with alkaline solutions. The process begins by dissolving fly ash particles using the high-alkaline solution. Then, the polymerization process occurs and eventually precipitates from the solution, forming the product phase. At the same time, precipitation occurs and eventually creates a three-dimensional solid matrix. The main outcome of this geopolymeric reaction is a sodium-aluminosilicate gel (Kovalchuk et al., 2008), (Ryu et al., 2013).

Fly ash has been widely applied in composite cement (Agrawal et al., 2019) (Lahoti et al., 2018). Most previous studies used fly ash as a precursor in geopolymer cement. Fly ash that will be utilized as the precursor in geopolymer must be characterized completely to determine the fly ash's ability in producing geopolymerization. This study investigated the possibility of using the fly ash from the Power Plant in Nagan Raya, Aceh Province, Indonesia. This article reports the characterization results of fly ash, the compressive strength of the geopolymeric material produced, and geopolymerization.

Low calcium fly ash is commonly used in geopolymer because it has a better setting time, even though high-calcium fly ash is abundant and harmful to the environment. High-calcium fly ash is rarely used due to its poor characteristics to be applied as a base material for geopolymer concrete (Diaz et al., 2010; Guo et al., 2010; Rattanasak et al., 2011; Temuujin et al., 2014; Tho-in et al., 2012). The high calcium content in fly ash makes the geopolymer concrete harden too fast; thus, it is challenging to implement it as a large-scale construction material. Fly ash from the Nagan Raya Power Plan is high calcium fly ash. To utilize local

resources as a source of construction material, fly ash from the Nagan Raya power plant must be examined for its feasibility on geopolymer cement.

This paper focuses on studying fly ash properties as a precursor in the cement composite binder for geopolymers. This study aims to examine the raw material characteristics of fly ash as the material for geopolymer cement. Besides, this research also assessed the geopolymerization produced by geopolymer cement. The characterization assessment of the waste materials, such as fly ash, informs the feasibility of the material as a construction material. It can also provide an opportunity to mitigate the disposal and its associated environmental impacts.

Material and Methods
Materials

This study used high calcium fly ash from the Nagan Raya power plant in Aceh Province, Indonesia (NFA). The NFA had specific gravity and average particle sizes of 2.457 and 30 μm, respectively. Fly ash was prepared by first passing it through 200 mesh. It was physically activated at 105 °C for one hour to evaporate the water and impurities in its pores. Table 1 displays the chemical compositions of the NFA. The liquid portion in the mixture consisted of 10 M sodium hydroxide (NaOH) (99% purity- Merck) and sodium silicate (Na_2SiO_3), with 12.81% Na_2O, 24.19% SiO_2, and 63% H_2O. The Epoxy resin used was made in America, which was purchased from the Indonesia Chemical Reagent Company. All chemicals were purchased from Indonesia Chemical Reagent Company and were used without further purification.

Mix Proportion

The process of mixing geopolymer paste was conducted by preparing the materials shown in Table 1. NaOH solution was made of 10 Molar NaOH mixed with Na_2SiO_3 and then left for 24 hours so that the solution was completely mixed into an alkaline solution. Figure 1 showed the specimen preparation process. In the first step, fly ash was mixed with an alkaline solution and stirred for 20 minutes. The epoxy resin was mixed after the geopolymerization process was complete. Next was molding and curring, in which the paste was put into a 5x5x5 cm cube mold and treated at room temperature. After three days, the paste was removed from the mold.

Table 1. Mix proportion of geopolymer pastes

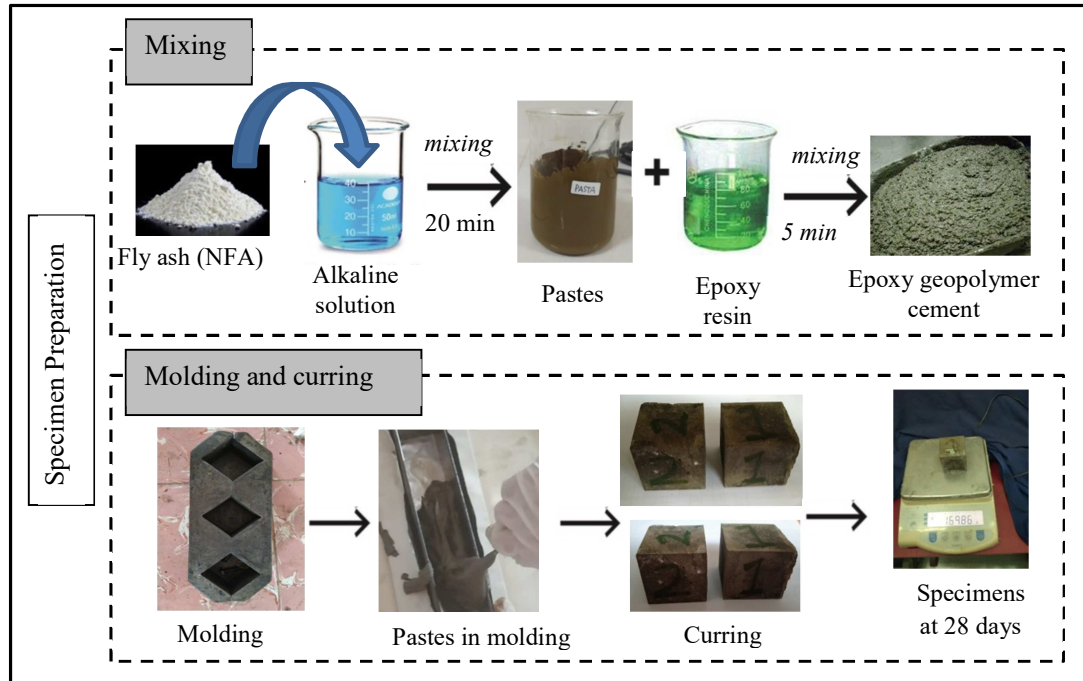| NFA (g)	NaOH (g)	Na_2SiO_3 (g)	Water (ml)	Epoxy Resin (g)	Na_2SiO_3/NaOH Ratio
90	14	14	35	31	1

Figure 1. The preparation procedures for the specimen in this study

Testing Procedures

Hydrometer Method

The hydrometer method part ASTM D7928 was used to determine the particle size distribution used. It was performed by calculating the size of soil particles from the speed they settle in a liquid suspension. The results showed that the particle size distribution of soil is finer than the 75µm sieve.

Scanning Electron Microscopy (SEM)

A scanning electron microscope (SEM) microscopy study was carried out to classify the microstructural characteristics of fly ash and geopolymerization. The microscopy analysis was done using Field Electron and Ion Company, Hillsboro, and Oregon. The specimen with double stick carbon tape was mounted on a brass stub sample holder. Using a blazer sputtering coater, the specimen was dried using infrared light for five minutes and then coated between 20–25A thick. The micrographs were registered at 15 kV and 5000x magnification.

Fourier Transform Infrared (FTIR) Spectroscopy

After 28 days, geopolymer cement paste samples were cut into thin slices, then grounded into fine particles, and filtered using a 75-µm sieve to obtain the required powder samples for FTIR tests. Fourier transform infrared (FT-IR) absorption spectra were recorded in the range of $4,000-450$ cm^{-1}. Spectra were recorded at a spectral resolution of 4 cm^{-1}, a scan speed of 0.2 cm/s, and they were analyzed with Spectrum software.

X-Ray Diffraction (XRD)

Quantitative XRD analysis was conducted consistently using the Reference Intensity Method (RIM) described by Chung (Chung, 1974). The XRD scans were performed at 10 to 50° 2θ with a 0.5 s/step scan speed. The phases of the NFA and geopolymer paste at 28 days were determined by XRD analysis.

The crystallinity index (Crl) used is decided based on the reflected depth data following the means of Segal (1959).

$$Crl~(\%) = \frac{I_{002} - I_{am}}{I_{002}} \times 100 \quad \ldots\ldots\ldots\ldots\ldots\ldots\ldots\ldots\ldots(1)$$
$$Amorphous~phase~(\%) = 100 - \Sigma~Crl. \quad \ldots\ldots\ldots\ldots\ldots(2)$$

Where I_{002} is the maximum intensity of the (002) lattice diffraction peak, and I_{am} is the intensity scattered by the amorphous part of the sample. The diffraction peak for the plane (002) is located at the diffraction angle 2θ = 22°, and the intensity is at the diffraction angle 2θ=18°.

Compressive Strength

The compressive strength test was performed on the 50 mm^3 paste specimens based on ASTM C109 using a Technotest concrete testing machine. The reported seven days and 28 days compressive strength values are the average of three samples for each mix design.

Results and Discussion
Characterization of Fly Ash
Chemical Characterization

To determine the quality of fly ash used in this study, the NFA was compared to several fly ash from other countries. The NFA was compared to fly ash from Sarawak (SFA) and fly ash from Glastone, Australis (GFA), to assess its mineralogical.

The chemical compositions of fly ash types were examined using X-ray Fluorescence Spectrometer (XRF), and the results are shown in Table 2.

Table 2. Chemical compositions of fly ash

Elements (%)	Nagan Raya fly ash (NFA)	Sarawak fly ash (SFA) (Leong et al., 2016)	Gladstone fly ash (GFA) (Leong et al., 2016)	Ordinary portland cement (OPC) (Sutan et al., 2014)
SiO_2	21.07	43.8	51.1	21.8
Al_2O_3	9.65	18.1	25.7	5.8
Fe_2O_3	27.23	7.7	12.5	3.3
CaO	32.58	3.9	4.3	63.0
MnO	0.44	22.8	0.2	-
K_2O	1.17	2.0	0.7	0.3
SO_3	5.69	0.1	0.2	2.4
TiO_2	1.68	0.6	1.3	-
Cl	0.22	-	-	

Elements (%)	Nagan Raya fly ash (NFA)	Sarawak fly ash (SFA) (Leong et al., 2016)	Gladstone fly ash (GFA) (Leong et al., 2016)	Ordinary portland cement (OPC) (Sutan et al., 2014)
Ag_2O	0.23	-	-	
Yb_2O_3	0.09	-	-	
P_2O_5		0.1	0.9	-
MgO		0.5	1.5	2.0
Na_2O		0.3	0.8	0.5
LOI		0.5	0.6	1.0

According to ASTM C618, fly ash classification is divided into two classes: class F and class C; the main differences between these classes are the amount of calcium, silica, aluminum, and iron oxide in them. Class F fly ash consists of <10% CaO. Table 2 shows that the largest composition of NFA is CaO, Fe_2O_3, and SiO_2. Both SFA and GFA are classified as class F fly ash, while and NFA is class C.

Based on the visual observation, NFA is gray, SFA is darker in the shade (i.e., gray color), and GFA is brownish, as shown in Figure 2.
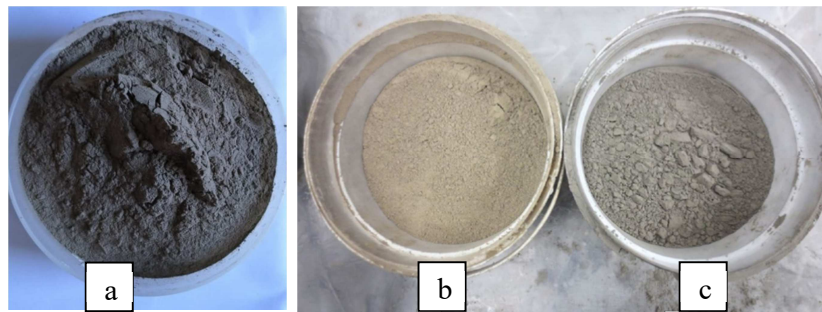

Figure 2. The physical appearance of (a) NFA-grey, (b) GFA-brownish, and (c) SFA-grey (lighter). The interpretation (b) and (c) are based on the reference (Leong et al., 2016).

Figure 2 showed that fly ash with a lighter color is produced from anthracite or bituminous coal and has a finer particle size. This color indicates better fly ash quality (Chindaprasirt et al., 2004), (Wattimena et al., 2017). The basicity index (Kb) and hydration modulus (HM) of NFA, SFA, and GFA are evaluated using the following equations.

$$Kb = \frac{CaO + MgO}{SiO_2 + Al_2O_3} \dots\dots\dots\dots\dots\dots\dots(3)$$

$$HM = \frac{CaO + MgO + Al_2O_3}{SiO_2} \dots\dots\dots\dots\dots\dots\dots(4)$$

The basicity index of NFA, SFA dan GFA, is 1.06, 0.08, and 0.07, respectively. The Kb of SFA and GFA is ≤1, indicating pozzolanic properties, quick lime, hydrated lime, or cement should be added to obtain cementitious properties. Meanwhile, the basicity index of NFA indicates pozzolanic and self-cementing

properties (no need to add lime). It contrasts with the self-cementing properties of SFA and GFA, which are very poor due to the lack of CaO content (Leong et al., 2016), (Wilińska & Pacewska, 2018).

The hydration modulus of NFA, SFA, and GFA is 2, 0.51, 0.62, respectively. This shows that the hydraulicity of the NFA is high, and it will harden faster, while it will take longer for the SFA and GFA to set.

Mineralogy

The mineralogy of NFA was studied based on the XRD test results, and the peaks represent the presence of the crystalline phases. The XRD result of NFA is similar to the corresponding XRD results of SFA and GFA, as shown in Figure 3. The dominant mineral observed in NFA, SFA, and GFA is quartz. NFA's highest peak was observed at approximately 26.65°at 2θ, suggesting that a greater amount of amorphous material was present. The XRD pattern of NFA shows the wider band from 25° to 30°. GFA band was ranged from 20° to 40°.
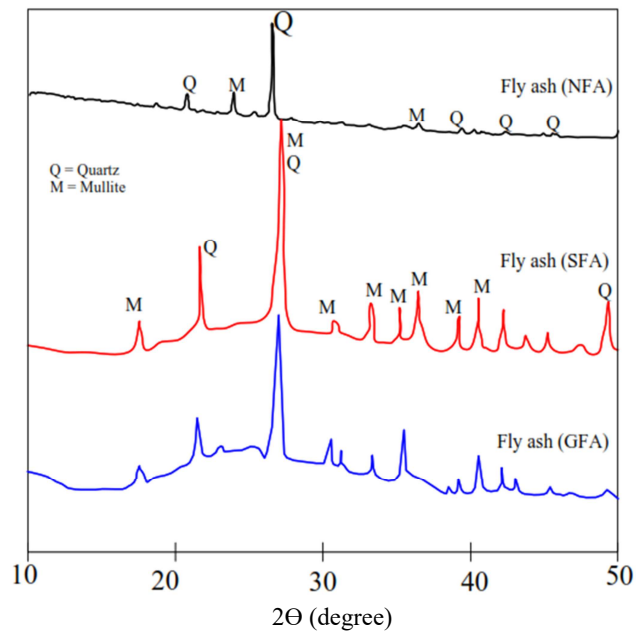

Figure 3. Result of X-ray diffraction (XRD) on NFA, SFA, and GFA. XRD on SFA and GFA from (Leong et al., 2016), re-drawn

Figure 3 showed that the results indicate that the amorphous nature of GFA is more prominent than NFA and SFA. The amorphous property of fly ash is due to the high temperature of coal combustion, which induces the material phase from crystalline to amorphous (Itskos et al., 2010) (Fuller et al., 2018). It is possible to dissolve more amorphous silica and alumina from fly ash and contribute to geopolymerization, thus creating a stronger geopolymer structure.

Eqs (1) and Table 3 show that NFA fly ash contains 64.91% crystalline, and the remaining is amorphous.

Table 3. The crystallinity of the fly ash sample (NFA)

Samples	2Θ (am)	I_{am}	2Θ (002) (°)	I_{002}	Crl (%)
Fly ash	26.26	4642	26.54	13230	64.91

The percentage of the amorphous part strongly correlates with the compressive strength. The more amorphous part in fly ash, the more SiO_2 is dissolved with alkaline solutions, and it increases the C-S-H gel needed in the geopolymer process (Azevedo et al., 2019), (Mohammed et al., 2019). Meanwhile, NFA only has a small amorphous portion (35.09%).

Particle Size Distribution

The particle size distribution in NFA is presented in Figure 4. While, Table 4 shows the results of the mean diameter and particle size distribution at 10% (d10), 50% (d50) and 90% (d90).
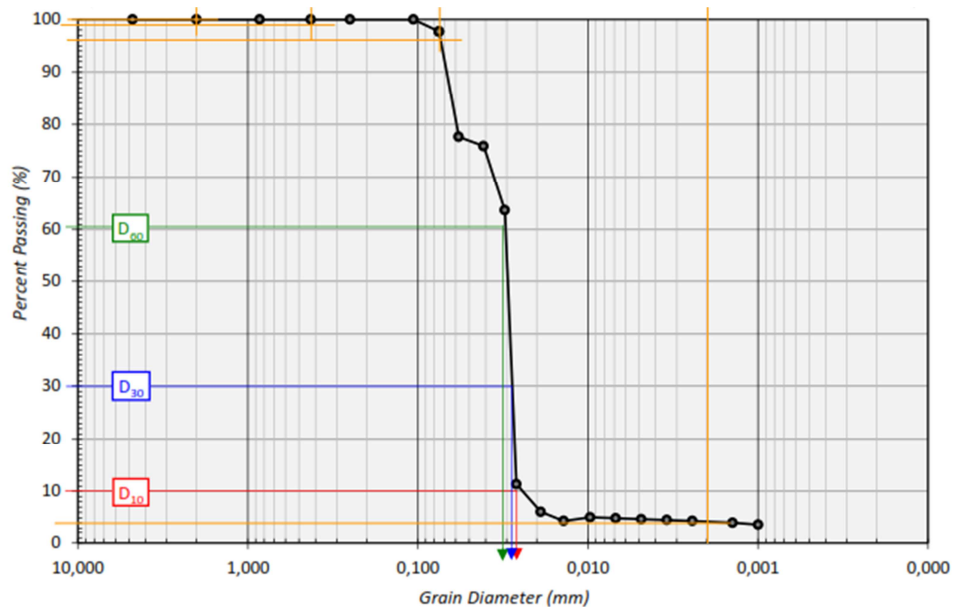

Figure 4. The particle size distribution of NFA

Figure 4 showed that based on the particle size analysis, it could be seen that the NFA fly ash particle size is mostly 0.074-0.002 mm (93.7%). Compared to the original Portland cement with 70% passing the 200 mesh, the NFA particle size is smoother, with 93.7% passing the 200 mesh. Smaller particle sizes will influence the higher hydration rate. Another advantage of smaller size is that the smoother cement, the less chance of bleeding, and the better workability. However, fine fly ash also has a drawback: the finer the fly ash, the greater the possibility of shrinkage and cracking. Hence, it is necessary to note in using NFA for binder materials in geopolymers.

Table 4. Particle size distribution

Mode	Particle size group (mm)	NFA (%)
Gravel	> 2	0
Fine sand	0.42 – 0.074	2.3
Silt	0.074 – 0.002	93.70
Clay	0.002	4

Table 5. Physical properties of NFA

Sample	NFA
Diameter at 10% (d_{10}) (mm)	0.028
Diameter at 30% (d_{30}) (mm)	0.03
Diameter at 60% (d_{60}) (mm)	0.04
Mean size (µm)	30
Specific gravity	2.457

The Coefficient of Curvature (Cc) and Coefficients of Uniformity (Cu) were also used to compare the variety of particle size gradation of fly ash, as given in Eqs. 5 and 6.

$$C_c = \frac{(D_{30})^2}{D_{10} \; x \; D_{60}} \quad …………………………………(5)$$

$$C_u = \frac{D_{60}}{D_{10}} \quad …………………………….…..……..(6)$$

Based on Table 5, the analysis revealed that Cu and Cc for NFA were 1.43 and 0.80, respectively. The NFA's Cu value is lower than those of SFA (9.4) and GFA (7.3), showing the NFA particle size is uniform and in a small range. A higher Cu value reflects a more non-uniform particle size distribution and broader ranges of particle sizes (Leong et al., 2016). In this case, the higher number of fine particles in the NFA increases the filler effect, although the structure formed tends not to be more compact and rigid.

Cc value shows the curvature degree of the plot for the particle size distribution. The Cc value of the NFA is 0.8 or close to 1, while it is between 1-3 for the SFA and GFA. These values indicate that the NFA, SFA, and GFA have a well-graded particle size distribution.

Scanning Electron Microscopy

Figure 5 showed an SEM image of NFA, SFA, and GFA. NFA fly ash particles, as seen in the SEM micrographs, are very small. Figures 5a and b showed the distribution of NFA fly ash looks uniform. The distinct particle size distribution between large and small particles is evident on the NFA. Figure 5c-f showed the particles' sizes of

SFA and GFA are distributed equally. From a workability point of view, the shape of NFA fly ash particles that are less spherical will increase the internal friction. The irregular particles will increase absorption ability and fluid demand (Lynn et al., 2016). Therefore, a higher amount of aqueous solution is necessary to obtain better workability of NFA.
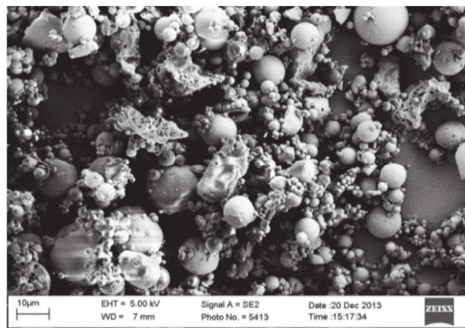
This is different from the SFA and GFA; both have a smooth spherical particle shape; the ball bearing and the lubricant effects are enhanced, improving the mixture's ability to work and flow.
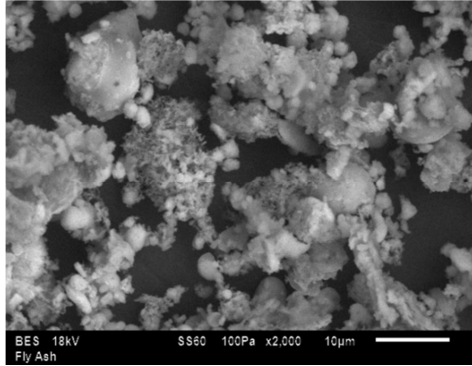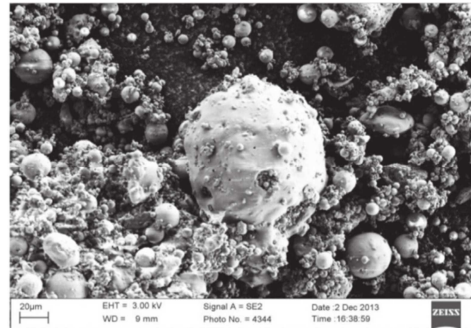

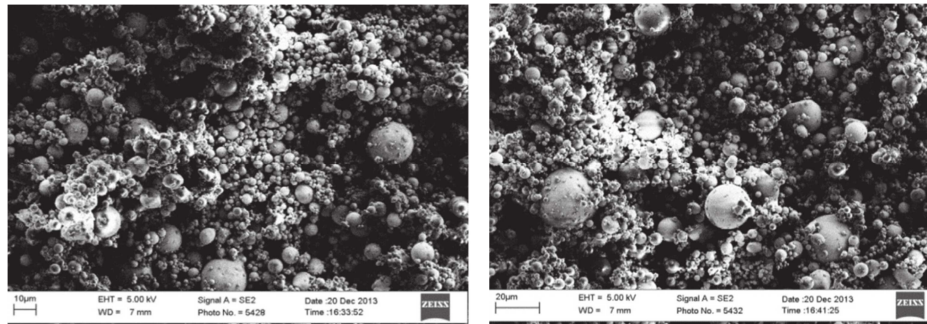(a) NFA-irregular grain (magnification to 10µm)
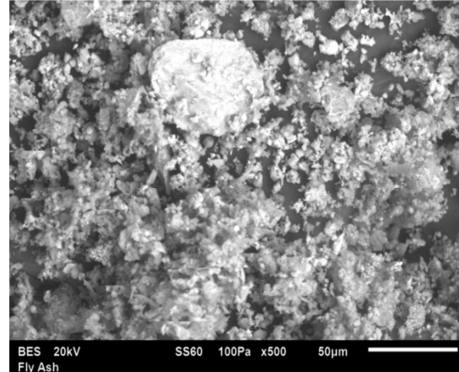
b) NFA- Irregular grains with some of them greater than other particles

(c) SFA-distribution from fine to coarser portions is evenly (magnification to 10µm). *Source:* (Leong et al., 2016)

(d) SFA-less spherical and appear with some angularities (magnification to 20 µm). *Source:* (Leong et al., 2016)

(e) GFA-distribution from fine to coarser portions is in decreasing order (magnification to 20µm). *Source:* (Leong et al., 2016)

(f) GFA-smooth sphere and spherical (magnification to 20µm). *Source:* (Leong et al., 2016)

Figure 5. SEM on NFA, SFA, and GFA

Compressive Strength and Microstructure of Geopolymer Cement
Compressive Strength

The compressive strength of the Geopolymer paste was tested after seven days and 28 days; the results are presented in Figure 6. The compressive strength shows an increase after 28 days (21.5 MPa). This compressive strength is slightly below the compressive strength reported by (Phoo-ngernkham et al., 2014; Saidi & Hasan, 2020).
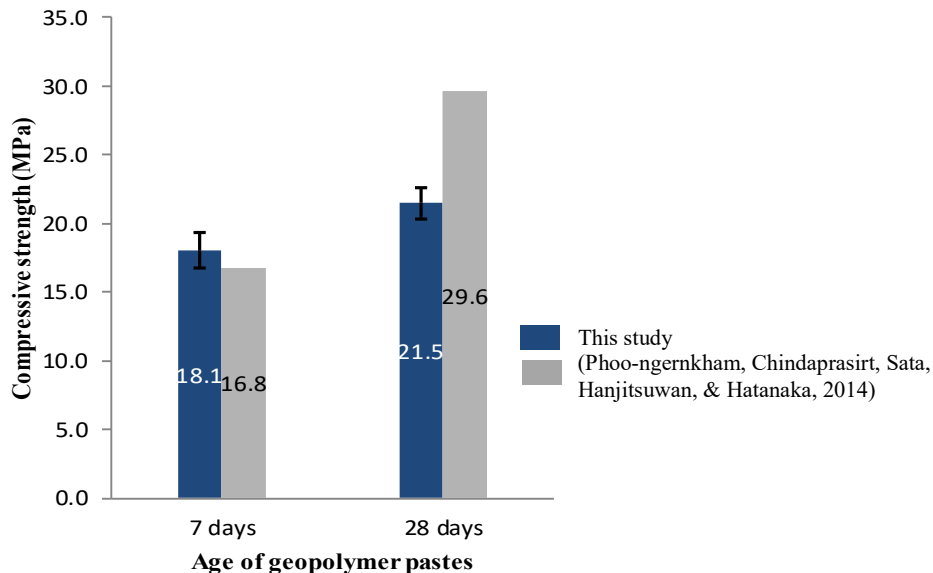

Figure 6. The compressive strength of geopolymer paste at 7 and 28 days

Structurally, geopolymer cement from the NFA had fulfilled the requirements of a geopolymer material. Epoxy resin can interact chemically with

geopolymer suspensions to create new chains consisting of $[AlO4]^{5-}$, $[SiO4]^{4-}$ tetrahedral, and polyamines (Du et al., 2016). Figure 7 showed the reaction of the epoxy resin with the geopolymer that occurred by OH- binding. This mixture showed an excellent dispersion to the micro-level with the increasing initial compressive strength.
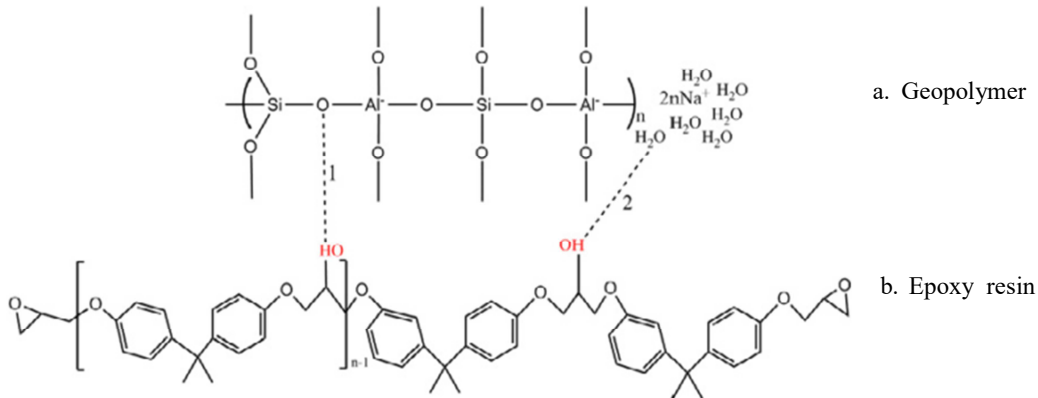

a. Geopolymer

b. Epoxy resin

Figure 7. The schematic interactions between geopolymer and the epoxy resin (Ferone et al., 2013).

X-Ray Diffraction Characterization

Figure 8 shows the XRD patterns of the NFA and the geopolymer cement containing 20 wt% of epoxy resin. A decrease in peak 2θ at 26.54° indicates that the amorphous part of the fly ash has transformed into a C-S-H solution on the geopolymer cement. The XRD graph shows a similar diffraction pattern between the NFA and geopolymer cement; only the peak at an angle of 2θ seems to decrease.

The amorphous part of fly ash is only 33.23%, but the results show that the amorphous part could be transformed into a C-S-H solution on the geopolymer cement. An increase in compressive strength also supports this.
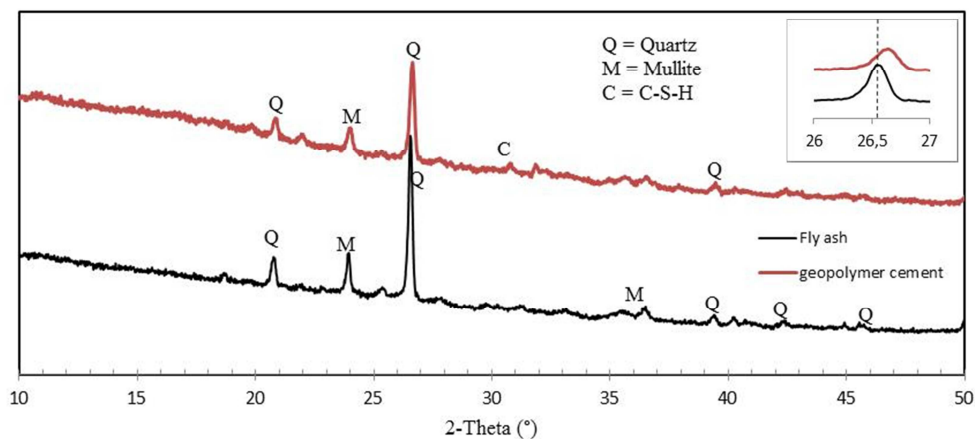

Figure 8. XRD of NFA and geopolymer cement at 28 days

FTIR Analysis

Figure 9 displays the FTIR spectra of the geopolymer-based epoxy and fly ash as raw material. The intensity of the peak at 521 cm^{-1} was associated with Si-O-Si bending vibration (Aouan et al., 2021),(Sarkar & Dana, 2021). The small band of fly ash at around 671 cm^{-1} represents the functional group of AlO_2, which is its chemical composition. The band of geopolymer pastes at about 795 cm^{-1} is characterized as the crystalline phase of quartz (Ranjbar et al., 2014), (Arioz et al., 2020). However, it only shows a small intensity at the fly ash band because the amorphous part of fly ash has been transformed into the crystalline phase. The wide vibration bands around 1145 cm^{-1} exhibited in spectra were attributed to T-O-Si (T: Si or Al) (Komnitsas et al., 2007) (Da Luz et al., 2019).

Consequently, other small bands at about 1,467 cm^{-1} that emerge in the geopolymer specimens are assigned to carbonate asymmetric stretching. The presence of sodium carbonate due to the atmospheric carbonation of alkaline O-C-O-O is indicated by this band (Lee & Deventer, 2002),(Erfanimanesh & Sharbatdar, 2020). The wide vibration bands around 1,703 and 3,629 cm^{-1} exhibited in spectra were attributed to O-H stretching and bending, respectively (Gharzouni et al., 2016) (Gouny et al., 2012), (Troëdec et al., 2009). It is predicted that epoxy contributed to these bonds as interactions between geopolymer and the epoxy resin. Another band was around 1,145 cm^{-1}, corresponding to the Si-O-Al and Si-O-Si vibration bands of the geopolymer. This band is a major fingerprint for the geopolymer matrix and defines the extent of polysialylation.
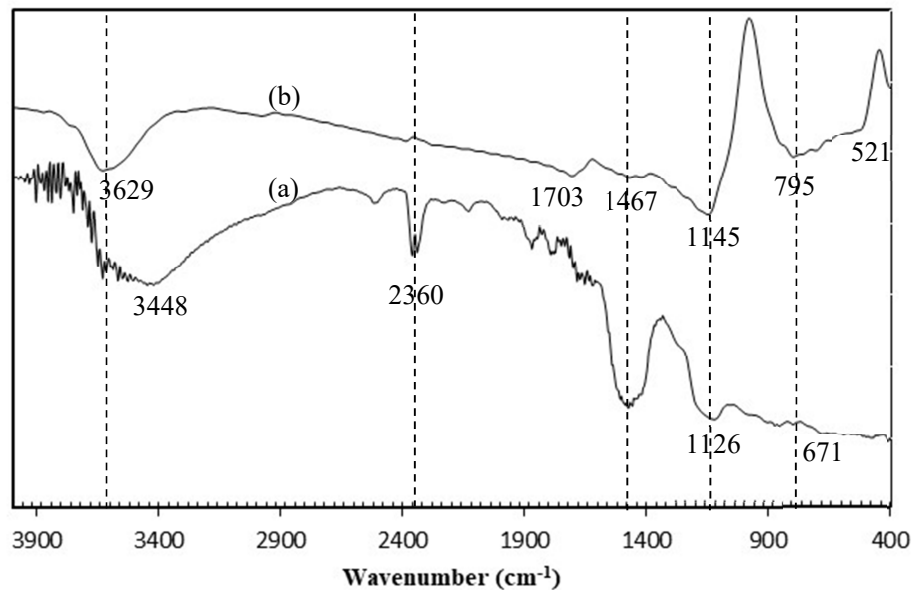

Figure 9. FTIR spectra of the geopolymer, (a) fly ash (b) geopolymer pastes

Figure 9 shows that several changes are observed when the values are compared to the same characteristic bands of NFA. The change of vibrational and deformation bands of Si-O-Si to high and low values is noticeable. At the vibration bands of 950-1,200 cm^{-1} attributed to T-O-Si (T: Si or Al) (Peyne et al., 2017),(Jose et al., 2020), it also seems to change. Besides, the NFA used as raw material for Si-O-Al shows a low intensity. Still, after the geopolymerization process, a C-S-H gel is formed, increasing the intensity of vibration bands. This result is consistent with the XRD analysis of geopolymer cement that shows the depolymerization. It indicates a decrease in peak 2θ at 26.54° and NFA transformed into a C-S-H solution.

Conclusion

This experimental study proves that geopolymers can be formed from high calcium fly ash from Nagan Raya. The NFA mineral indicates pozzolanic and self-cementing properties. However, NFA has some disadvantages. The hydration modulus of NFA is 2, so it will harden faster, and microstructural formed tends not to be more compact and rigid. Also, the percentage of the amorphous part of fly ash is 35.09%, affecting C-S-H gel formation; therefore, another additional material, epoxy resin, should be added to the hydroxyl bond. This study shows that epoxy can correct the weakness of NFA by contributing hydroxyl bonds to geopolymers. This aligns with XRD analysis results, indicating that NFA has transformed into a C-S-H solution on the geopolymer cement. These XRD results are also supported by FTIR analysis results showing a hydroxyl O-H bond at vibration bands around 1,703 and 3,629 cm^{-1}, which is estimated from the epoxy resin. The compressive strength shows an increase after 28 days (21.5 MPa), so that it is concluded that NFA can be used as a raw material in geopolymers.

Acknowledgement

References

Agrawal, U., Wanjari, S., & Naresh, D. (2019). Impact of replacement of natural river sand with geopolymer fly ash sand on hardened properties of concrete. *Construction and Building Materials*, *209*. https://doi.org/https://doi.org/10.1016/j.conbuildmat.2019.03.134

Aouan, B., Alehyen, S., Fadil, M., Alouani, M. EL, Khabbazi, A., Atbir, A., & Taibi, M. (2021). Compressive strength optimization of metakaolin-based geopolymer by central composite design. *Chemical Data Collections*, *31*, 100636. https://doi.org/https://doi.org/10.1016/j.cdc.2020.100636

Arioz, E., Arioz, O., & Kockar, O. M. (2020). Geopolymer Synthesis with Low Sodium Hydroxide Concentration. *Iranian Journal of Science and Technology, Transactions of Civil Engineering*, *44*, 525–533. https://doi.org/https://doi.org/10.1007/s40996-019-00336-1

Azevedo, A. G. S., Strecker, K., Barros, L. A., Tonholo, L. F., & Lombardi, C. T. (2019). Effect of Curing Temperature, Activator Solution Composition and Particle Size in Brazilian Fly-Ash Based Geopolymer Production. *Materials Research*, *22*. https://doi.org/https://doi.org/10.1590/1980-5373-mr-2018-0842

Chindaprasirt, P., Homwuttiwong, S., & Sirivivatnanon, V. (2004). Influence of fly ash fineness on strength, drying shrinkage and sulfate resistance of blended cement mortar. *Cement and Concrete Research*, *34*(7), 1087–1092. https://doi.org/10.1016/j.cemconres.2003.11.021

Chung, F. H. (1974). Quantitative Interpretation of X-ray Diffraction Patterns of Mixtures. I1. Adiabatic Principle of X-ray Diffraction Analysis of Mixtures. *J. Appl. Crystallogr*, *7*, 526–530.

Da Luz, G., Gleize, P. J. P., Batiston, E. R., & Pelisser, F. (2019). Effect of pristine and functionalized carbon nanotubes on microstructural, rheological, and mechanical behaviors of metakaolin-based geopolymer. *Cement and Concrete Composites*, *104*(July 2018), 103332. https://doi.org/10.1016/j.cemconcomp.2019.05.015

Diaz, .I., Allouche, E. N., & Eklund, S. (2010). Factors affecting the suitability of fly ash as source material for geopolymers. *Fuel*, *89*(5), 992–996. https://doi.org/https://doi.org/10.1016/j.fuel.2009.09.012

Du, J., Bu, Y., Shen, Z., Hou, X., & Huang, C. (2016). Effects of epoxy resin on the mechanical performance and thickening properties of geopolymer cured at low temperature. *Materials and Design*, *109*, 133–145. https://doi.org/10.1016/j.matdes.2016.07.003

Erfanimanesh, A., & Sharbatdar, M. K. (2020). Mechanical and microstructural characteristics of geopolymer paste, mortar, and concrete containing local zeolite and slag activated by sodium carbonate. *Journal of Building Engineering*, *32*, 101781. https://doi.org/https://doi.org/10.1016/j.jobe.2020.101781

Ferone, C., Roviello, G., Colangelo, F., Cioffi, R., & Tarallo, O. (2013). Novel hybrid organic-geopolymer materials. *Applied Clay Science*, *73*(1), 42–50. https://doi.org/10.1016/j.clay.2012.11.001

Fuller, A., Maier, J., Karampinis, E., Kalivodova, J., Grammelis, P., Kakaras, E., & Scheffknecht, G. (2018). Fly Ash Formation and Characteristics from (co-) Combustion of an Herbaceous Biomass and a Greek Lignite (Low-Rank Coal) in a Pulverized Fuel Pilot-Scale Test Facility. *Energies*, *11*(6), 1–38. https://doi.org/https://doi.org/10.3390/en11061581

Gharzouni, A., Vidal, L., Essaidi, N., Joussein, E., & Rossignol, S. (2016).

Recycling of geopolymer waste: Influence on geopolymer formation and mechanical properties. *Materials & Design*, *94*, 221–229. https://doi.org/https://doi.org/10.1016/j.matdes.2016.01.043

Gouny, F., Fouchal, F., Maillard, P., & Rossignol, S. (2012). A geopolymer mortar for wood and earth structures. *Construction and Building Materials*, *36*, 188–195. https://doi.org/https://doi.org/10.1016/j.conbuildmat.2012.04.009

Guo, X., Shi, H., Chen, L., & Dick, W. A. (2010). Alkali-activated complex binders from class C fly ash and Ca-containing admixtures. *Journal of Hazardous Materials*, *173*(1), 480–486. https://doi.org/https://doi.org/10.1016/j.jhazmat.2009.08.110

Itskos, G., Itskos, S., & Koukouzas, N. (2010). Size fraction characterization of highly-calcareous fly ash. *Fuel Processing Technology*, *91*(11), 1558–1563. https://doi.org/https://doi.org/10.1016/j.fuproc.2010.06.002

Jose, A., Nivitha, M. R., Krishnan, J. M., & Robinson, R. G. (2020). Characterization of cement stabilized pond ash using FTIR spectroscopy. *Construction and Building Materials*, *263*(10), 120136. https://doi.org/https://doi.org/10.1016/j.conbuildmat.2020.120136

Komnitsas, K., Zaharaki, D., & Perdikatsis, V. (2007). Geopolymerisation of low calcium ferronickel slags. *J Mater Sci*, *42*, 3073–3082. https://doi.org/10.1007/s10853-006-0529-2

Kovalchuk, G., Jiménez, A. F., & Palomo, A. (2008). Alkali-activated fly ash. Relationship between mechanical strength gains and initial ash chemistry. *Materiales de Construcción*, *58*(291), 35–52. https://doi.org/https://doi.org/10.3989/mc.2008.v58.i291.101

Lahoti, M., Wong, K. K., Tan, K. H., & Yang, E.-H. (2018). Effect of alkali cation type on strength endurance of fly ash geopolymers subject to high temperature exposure. *Materials & Design*, *154*, 8–19. https://doi.org/https://doi.org/10.1016/j.matdes.2018.05.023

Leong, H. Y., Ong, D. E. L., Sanjayan, J. G., & Nazari, A. (2016). Suitability of Sarawak and Gladstone fly ash to produce geopolymers: A physical, chemical, mechanical, mineralogical and microstructural analysis. *Ceramics International*, *42*(8), 9613–9620. https://doi.org/10.1016/j.ceramint.2016.03.046

Lynn, C. J., OBE, R. K. D., & Ghataora, G. S. (2016). Municipal incinerated bottom ash characteristics and potential for use as aggregate in concrete. *Construction and Building Materials*, *127*(30), 504–517. https://doi.org/https://doi.org/10.1016/j.conbuildmat.2016.09.132

Mohammed, B. S., Haruna, S., Wahab, M. M. A., Liew, M. S., & Haruna, A. (2019). Mechanical and microstructural properties of high calcium fly ash one-part geopolymer cement made with granular activator. *Heliyon*, *5*(9), e02255. https://doi.org/https://doi.org/10.1016/j.heliyon.2019.e02255

Peyne, J., Gautron, J., Doudeau, J., Joussein, E., & Rossignol, S. (2017). Influence of calcium addition on calcined brick clay based geopolymers: A thermal and FTIR spectroscopy study. *Construction and Building Materials*, *152*(15), 794–803. https://doi.org/https://doi.org/10.1016/j.conbuildmat.2017.07.047

Phoo-ngernkham, T., Chindaprasirt, P., Sata, V., Hanjitsuwan, S., & Hatanaka, S. (2014). The effect of adding nano-SiO2 and nano-Al2O3 on properties of high calcium fly ash geopolymer cured at ambient temperature. *Materials and Design*, *55*, 58–65. https://doi.org/10.1016/j.matdes.2013.09.049

Ranjbar, N., Mehrali, M., Behnia, A., Alengaram, U. J., & Jumaat, M. Z. (2014). Compressive strength and microstructural analysis of fly ash/palm oil fuel ash based geopolymer mortar. *Materials & Design*, *59*, 532–539. https://doi.org/https://doi.org/10.1016/j.matdes.2014.03.037

Rattanasak, U., Pankhet, K., & Chindaprasirt, P. (2011). Effect of chemical admixtures on properties of high-calcium fly ash geopolymer. *International Journal of Minerals, Metallurgy, and Materials*, *18*(3), 364. https://doi.org/https://doi.org/10.1007/s12613-011-0448-3

Ryu, G. S., Lee, Y. B., Koh, K. T., & Chung, Y. S. (2013). The mechanical properties of fly ash-based geopolymer concrete with alkaline activators. *Construction and Building Materials*, *47*, 409–418. https://doi.org/DOI: 10.1016/j.conbuildmat.2013.05.069

Saidi, T., & Hasan, M. (2020). The effect of partial replacement of cement with diatomaceous earth (DE) on the compressive strength and absorption of mortar. *Journal of King Saud University - Engineering Sciences*. https://doi.org/10.1016/j.jksues.2020.10.003

Sarkar, M., & Dana, K. (2021). Partial replacement of metakaolin with red ceramic waste in geopolymer. *Ceramics International*, *47*(3). https://doi.org/https://doi.org/10.1016/j.ceramint.2020.09.191

Sutan, N. M., Yakub, I., & Hamdan, S. (2014). Physico characterization of polymer composite cement systems. In *High Performance and Optimum Design of Structures and Materials* (p. 103). WITPress.

Temuujin, J., Minjigmaa, A., Davaabal, B., Bayarzul, U., Ankhtuya, A., Jadambaa, T., & MacKenzie, K. J. D. (2014). Utilization of radioactive high-calcium Mongolian flyash for the preparation of alkali-activated geopolymers for safe use as construction materials. *Ceramics International*, *40*(10), 16475–16483. https://doi.org/https://doi.org/10.1016/j.ceramint.2014.07.157

Tho-in, T., Sata, V., Chindaprasirt, P., & Jaturapitakkul, C. (2012). Previous high-calcium fly ash geopolymer concrete. *Construction and Building Materials*, *30*, 366–371. https://doi.org/https://doi.org/10.1016/j.conbuildmat.2011.12.028

Troëdec, M., Peyratout, C. S., Smith, A., & Chotard, T. (2009). Influence of various chemical treatments on the interactions between hemp fibres and a lime matrix. *Journal of the European Ceramic Society*, *29*(10), 1861–1868.

https://doi.org/https://doi.org/10.1016/j.jeurceramsoc.2008.11.016

Wattimena, O. K., Antoni, A., & Hardjito, D. (2017). A review on the effect of fly ash characteristics and their variations on the synthesis of fly ash based geopolymer. *AIP Conference Proceeding, 1887*, 020041. https://doi.org/http://dx.doi.org/10.1063/1.5003524

Wilińska, I., & Pacewska, B. (2018). Influence of selected activating methods on hydration processes of mixtures containing high and very high amount of fly ash. *Journal of Thermal Analysis and Calorimetry*, *133*, 823–843. https://doi.org/https://doi.org/10.1007/s10973-017-6915-y